[논 문] - 비파괴검사학회지
Journal of the Korean Society for Nondestructive Testing
Vol. 26, No. 1 (2006. 2)

Use of the Mass-Spring Lattice Model for Simulation of Ultrasonic Waves in Austenitic Welds

Eunsol Baek*,† and Hyunjune Yim*

Abstract Feasibility is studied for an application of the mass-spring lattice model (MSLM), a numerical model previously developed for unidirectional composites, to the numerical simulation of ultrasonic inspection of austenitic welds modeled as transversely isotropic. Fundamental wave processes, such as propagation, reflection, refraction, and diffraction of ultrasonic waves in such an inspection are simulated using the MSLM. All numerical results show excellent agreement with the analytical results. Further, a simplified model of austenitic weld inspection has been successfully simulated using the MSLM. In conclusion, a great potential of the MSLM in numerically simulating ultrasonic inspections of austenitic welds has been manifested in this work, though significant further efforts will be required to develop a model with field practicality.

Keywords: Ultrasonic testing modeling, Numerical simulation, Mass-spring lattice model, Anisotropic welds

1. Introduction

Austenitic welds in many components of a nuclear power plant have been known difficult to inspect using the ultrasonic nondestructive testing method. This is mainly because those welds are anisotropic and inhomogeneous in their elastic properties, which may be attributed to non-uniform cooling during the formation of the weld. Propagation and scattering of ultrasonic waves in anisotropic media are much more complex than and much different from those in isotropic media. Therefore, to correctly interpret ultrasonic test results of an anisotropic austenitic weld, thorough understanding of wave phenomena therein is crucial.

A considerable number of studies have addressed ultrasonic wave phenomena in anisotropic austenitic welds. A noteworthy example is the series of work done by Ogilvy (1985; 1986). She used the ray method to trace the ultrasonic energy flow, and focused on finding the "optimal" direction of ultrasonic energy transmission for a given region of inspection. The ray method, however, cannot account for the effects of diffraction from discontinuities such as cracks which are often major targets of ultrasonic investigation. In addition, Langenberg et al. (2000) used Huyghens' principle in conjunction with the elastodynamic finite integration technique to model various wave phenomena involved in ultrasonic testing of anisotropic welds, and compared the numerical results with experiments. Yamawaki and Saito (2000) developed a convenient finite difference method based on the nodal calculation method, and applied it to simulate various wave phenomena including point-source wave generation in anisotropic media, and reflection and refraction in layered anisotropic media.

The present paper investigates the feasibility of using the mass-spring lattice model (MSLM) to simulate ultrasonic testing of anisotropic austenitic welds. The MSLM has successfully been used for simulation of ultrasonic waves, mostly in isotropic media (Yim and Sohn, 2000; Yim and Choi, 2000).

Received: October 7, 2005. Accepted: November 22, 2005. * Dept. of Mechanical Engineering, Hongik University, † Corresponding author: Dept. of Mechanical Engineering, Hongik University, Seoul, 121-791 (E-mail: ga3311602@wow1.hongik.ac.kr)

A slightly modified version of MSLM for transversely isotropic media (such as unidirectional composites) is used to simulate various fundamental problems related to the propagation and scattering of ultrasonic waves in austenitic welds. The computed wavefields are compared with the analytical solutions, if any. Based on the results, the potential for the use of this model in simulating ultrasonic inspection of austenitic welds is discussed.

2. Problem Definition and Numerical Model

Problems to be dealt with in this paper are defined here. A two-dimensional schematic diagram for the actual ultrasonic testing of an austenitic weld is shown in Fig. 1. Ultrasonic wave emitted from the transducer in Fig. 1 will undergo the following four fundamental processes: propagation, free-boundary reflection, reflection/refraction at material interface, and scattering from cracks. Therefore, this paper, as a preliminary study, investigates the capability of the MSLM, described below, to accurately simulate each of these fundamental processes.

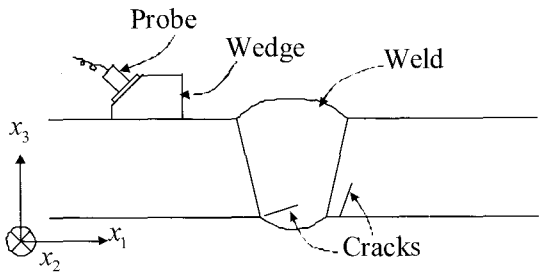

Fig. 1 Two-dimensional schematic diagram for ultrasonic testing of welds

Simplifying assumptions are made as to the material properties of the austenitic weld. The properties within the actual weld are assumed to be uniform, though they are not in reality. In addition, the elastic properties of the weld are assumed to be transversely isotropic, with the axis of symmetry oriented along the x_3-axis in Fig. 1. The elastic constants and density of the transversely isotropic austenite are adopted from Ogilvy (1986) as listed in Table 1. Furthermore, only two-dimensional problems are considered mainly because the numerical model used in this study is two-dimensional at its current stage of development. The plane of interest is taken as the $x_1 - x_3$ plane in Fig. 1, an orthogonal plane of the transversely isotropic weld.

Table 1 Material properties of transversely isotropic austenitic weld

Property	Values
C_{11}	26.3×10^{10} [N/m^2]
C_{12}	9.8×10^{10} [N/m^2]
C_{13}	14.5×10^{10} [N/m^2]
C_{33}	21.6×10^{10} [N/m^2]
C_{44}	12.9×10^{10} [N/m^2]
C_{66}	8.25×10^{10} [N/m^2]
ρ	7900 [kg/m^3]

Now, the numerical model to be used in this study is introduced. The model is a two-dimensional MSLM, based on the assumption of plane-strain states. The MSLM is a numerical model that consists of lumped masses representing the body's inertia, and springs representing its elasticity (Yim and Sohn, 2000). The MSLM to be mostly used in this study is the one, shown in Fig. 2, which was developed for transversely isotropic media, particularly for unidirectional composites (Yim and Choi, 2000). Note that the mesh sizes in the horizontal and vertical directions in Fig. 2 are set differently because the wave velocity in anisotropic media varies as a function of its propagating direction. The difference equations may easily be obtained by establishing the dynamic governing equations for the center mass in Fig. 2 as functions of the relative displacements of all adjacent masses (Yim and Choi, 2000). The horizontal and vertical grid spacings, h_1 and h_2 in Fig. 2, are determined such that $h_1/\Delta t$ and $h_2/\Delta t$ equal the fastest wave speeds in the two directions, respectively, where Δt is the time step whose value is typically chosen as 1/20 of one period for harmonic waves (Yim and Sohn, 2000).

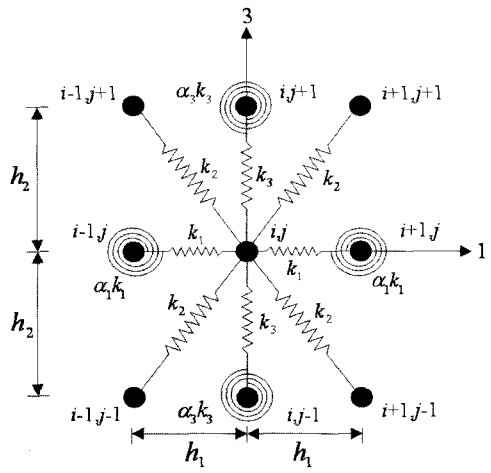

Fig. 2 Two-dimensional mass-spring lattice model developed for transversely isotropic media

3. Numerical Simulation

Each of the fundamental processes listed above, that is, propagation, free-boundary reflection, refraction at material interface, and scattering from a crack, is simulated using the MSLM. The computed wavefields are presented, and comparisons with analytical results, if any, are given in this section.

3.1. Generation and Propagation of Waves

First of all, waves generated from a point source are simulated. The source is modeled as a lumped mass, at the center of the medium, subjected to a one-cycle sinusoidal force in the horizontal direction, as indicated in Fig. 3(a). The frequency of this and all the following sinusoidal excitations throughout this study is set to 5 MHz. Computed wavefield for this case is shown in Fig. 3(b). In all figures of numerical results throughout this study, the brightness of each point (or pixel) represents the magnitude of displacement at that pixel, on a gray scale.

The analytically obtained wave surfaces (Musgrave, 1954; 1970) shown in Fig. 4 may directly be compared with the numerical results shown in Fig. 3(b). This is because a wave surface may be

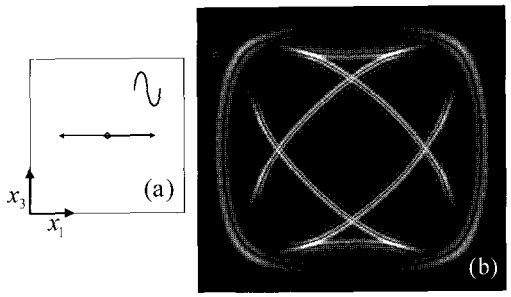

Fig. 3 Waves generated from point sources: (a) schematic diagram of problem; (b) numerical result

regarded as composed of infinitesimal plane wave segments, having wave normals in all directions, emitted from the origin of the coordinate system. It is well known that transversely isotropic media may support three different modes of waves: quasi-longitudinal (qP), quasi-shear vertical (qSV), and quasi-shear horizontal (qSH), where "quasi" emphasizes that their particle displacements are neither perpendicular nor parallel to the phase planes. Sections of the three corresponding wave surfaces in the $x_1 - x_3$ plane are shown in Fig. 4. Note the existence of cusps in the qSV wave surface. Taking into account the absence of qSH wave in the numerical results due to the plane-strain assumption, good agreement is observed between the analytical result and the corresponding numerical results.

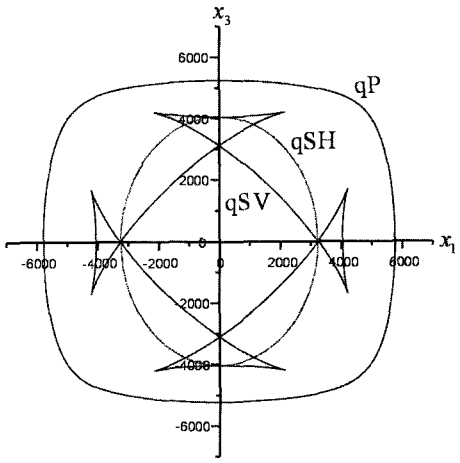

Fig. 4 Section of wave surfaces in $x_1 - x_3$ plane

Fig. 5 is for the case of line source excitation. In an attempt to generate purely qSV waves, we considered a line source (straight line segment in Fig. 5(a)) that has forces oriented in an oblique direction (parallel to the line segments with two arrowheads), which coincides with the displacement direction of the desired qSV wave. In all schematic diagrams in Figs. 5 through 16, this graphical notation holds. The numerical result shown in Fig. 5(b) shows the generation of a single qSV mode of wave. Further, the waves do not propagate in the direction normal to phase planes, but in oblique directions. This direction of wave propagation is indeed the direction of energy propagation, related to the group velocity vector. Three different directions shown in Fig. 5 represent the wave normal direction, the direction of particle displacement, and energy propagation direction, respectively. All these directions found numerically agree well with the corresponding directions found analytically.

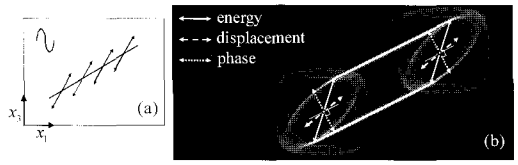

Fig. 5 Waves generated from line sources: (a) schematic diagram of problem; (b) numerical result

3.2. Reflection of Waves at Free Boundary

In this subsection, reflection of waves at free boundaries is considered in problems schematically shown in Figs. 6(a) and 7(a). Free boundaries are numerically modeled by imposing traction-free conditions, namely, $\sigma_{33} = \tau_{13} = 0$, written in the finite difference form. The angle of incidence is 18.4° in Figs. 6 and 7. Numerical results are given in Figs. 6(b) and 7(b), both showing expanded views of small regions along the lower free boundary where reflection occurs. In these problems, both qP and qSV waves (labeled RqP and RqSV, respectively) generated by the line sources are reflected with mode conversion.

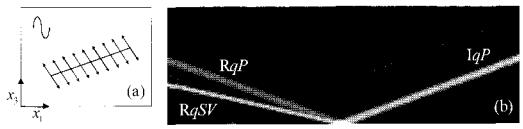

Fig. 6 Reflection of plane qP incident wave at 18.4°: (a) schematic diagram of problem; (b) numerical result

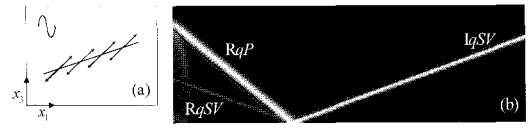

Fig. 7 Reflection of plane qSV incident wave at 18.4°: (a) schematic diagram of problem; (b) numerical result

The angle of reflection from a free boundary may analytically be calculated using the Snell's law, often by a graphical method based on the slowness surfaces (Henneke, 1972). For example, the angle of reflection may be determined by the following procedure, shown in Fig. 8 for the case of incident qP waves. Note that the s_1-axis in Fig. 8 coincides with the free boundary. First draw the slowness vector of the incident qP wave, $\mathbf{s}^{IqP}$, oriented by its angle of incidence, θ_1, and having its end at the origin of the slowness plane, as shown in Fig. 8. Then, draw a base vector, $\mathbf{b}$, defined as the projection of $\mathbf{s}^{IqP}$ on the s_1-axis, and draw a translated copy of $\mathbf{b}$ starting at the origin of the slowness plane. Now, extend a straight vertical (dot-dashed) line through the end point of the translated $\mathbf{b}$. Then, the intersections of this straight line with the slowness surfaces define the endpoints of the slowness vectors for the reflected waves. In the case of Fig. 8, one intersection (point A) with the qP surface and another (point B) with the qSV surface are found, resulting in the slowness vectors, $\mathbf{s}^{RqP}$ and $\mathbf{s}^{RqSV}$, for the reflected qP and qSV

waves. Therefore, it may be found that the angle of reflection for the reflected qP wave is equal to the angle of incidence, θ_1, whereas that for the reflected qSV wave is given by the angle, θ_2'. It should be mentioned here that a normal vector to a slowness surface at an intersection point (such as A and B in Fig. 8) defines the direction of energy propagation of the corresponding reflected wave, as indicated by the normalized group velocity vectors.

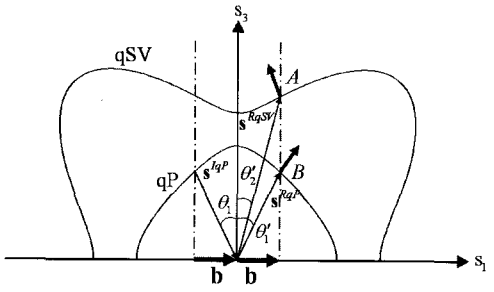

Fig. 8 Analytical determination of angles of reflection using slowness surfaces for incident qP waves

The graphical method shown in Fig. 8 for incident qP waves may similarly be applied to the cases of incident qSV waves (see Fig. 9) with some complications to be addressed below. Close examination of Fig. 9 reveals that there are two important values for the angle of qSV incidence: $\theta_{crit} = 28.8^\circ$ (called the critical angle) and $\theta_{tan} = 37.8^\circ$, at which the pertinent vertical lines (dotted lines a-a and b-b in Fig. 9) are tangent to the qP and qSV slowness surfaces, respectively. It may easily be observed from Fig. 9 that when the angle of qSV incidence is less than θ_{crit}, two reflected waves — one qP and the other qSV — are generated as in Fig. 7(b). Similarly, when the angle of incidence is between θ_{crit} and θ_{tan}, only one reflected qSV wave will result. This case is not further discussed because it occurs in isotropic media as well. The final case where the angle of incidence exceeds θ_{tan} is of particular interest. Consider, for example, the case of dotted vertical line c-c, corresponding to an angle of incidence, θ_2, in Fig. 9. In this case, two intersections with the qSV surface, giving slowness vectors $\mathbf{s}^{RqSV(1)}$ and $\mathbf{s}^{RqSV(2)}$, are found in the upper half plane of Fig. 9. Examining the associated energy propagation directions, however, the reflected qSV wave whose slowness vector is $\mathbf{s}^{RqSV(2)}$ turns out not to exist because its energy is directed toward the exterior of the medium as indicated by $\hat{\mathbf{c}}^{RqSV(2)}$. Searching for any other possible reflected waves as suggested by previous work (Henneke, 1972; Langenberg et al., 2000), two more intersections of the c-c line with the (dashed) qSV slowness surface in the lower half plane of Fig. 9, specified by $\mathbf{s}^{RqSV(3)}$ and $\mathbf{s}^{RqSV(4)}$, are considered. Of these two, the reflected qSV wave associated with $\mathbf{s}^{RqSV(3)}$ is expected to exist because its energy propagates toward the medium as indicated by $\hat{\mathbf{c}}^{RqSV(3)}$. Therefore, two reflected qSV waves, corresponding to $\mathbf{s}^{RqSV(1)}$ and $\mathbf{s}^{RqSV(3)}$ with angles of reflection $\theta_{2(1)}'$ and $\theta_{2(3)}'$ in Fig. 9, are expected to exist in numerical results, and they indeed manifest themselves (RqSV(1) and RqSV(3)) in Fig. 10, where the angle of the qSV incidence is $\theta_2 = 47^\circ$.

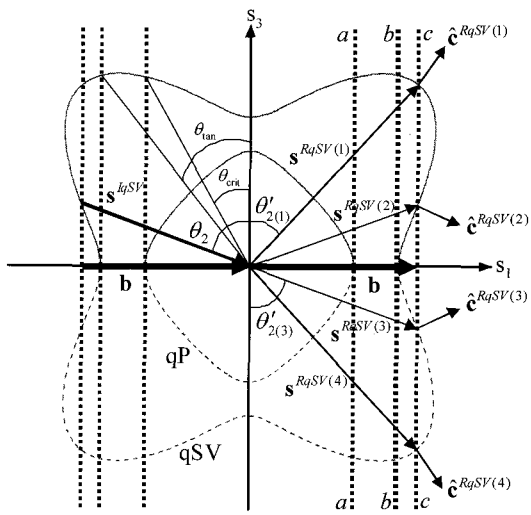

Fig. 9 Analytical determination of angles of reflection using slowness surfaces for incident qSV waves

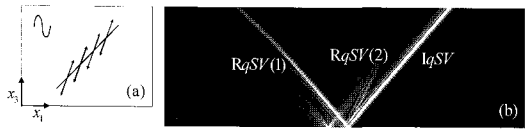

Fig. 10 Reflection of plane qSV incident wave at 47°: (a) schematic diagram of problem; (b) numerical result

Angles of reflection have been measured from the numerical results for various angles of incidence with incident qP and qSV waves. These numerically measured angles of reflection have shown excellent agreement (that is, within error of 0.5°) with the corresponding analytical values found by the graphical method shown in Figs. 8 and 9. Thus, the MSLM is proven to be capable of accurately simulating the reflection behavior of waves at free boundaries of transversely isotropic media.

3.3 Refraction of Waves at Material Interface

In the ultrasonic testing setup shown in Fig. 1, it is assumed that ultrasonic waves penetrate into the weld through the interface between the isotropic parent medium and the anisotropic weld (Ogilvy, 1985; 1986). In this study, the isotropic parent medium is taken to be ferrite, whose Lamé's elastic constants and density are set as $\lambda = 1.10\times10^{11}$ N/m^2, $\mu = 2.74\times10^{11}$ N/m^2, and $\rho = 7860$ kg/m^3, respectively.

Refraction of P and SV incident waves is considered in problems schematically depicted in Figs. 11(a) and 12(a), respectively, with angles of incidence of 45° and 20° with respect to the interface. The material interface has been modeled by imposing the continuity condition of tractions, σ_{13} and σ_{33}, across the interface. The numerical results given in Figs. 11(b) and 12(b) reveal that both qP and qSV refracted waves (labeled TqP and TqSV) are transmitted into the anisotropic weld at the same time as P and SV reflected waves (labeled RP and RSV) are generated and propagate back into the isotropic parent medium.

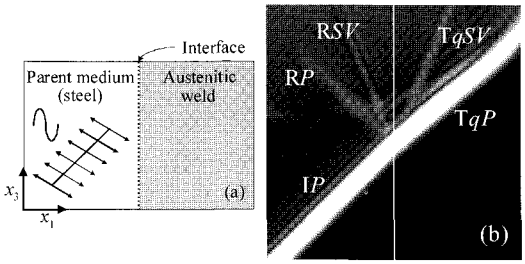

Fig. 11 Reflection and refraction of plane P incident wave at 45°: (a) schematic diagram of problem; (b) numerical result

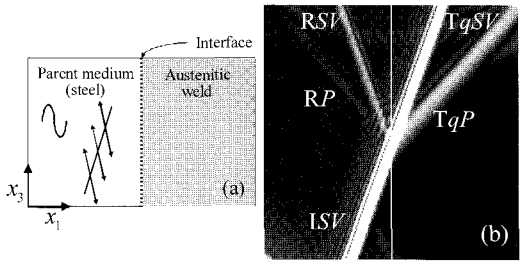

Fig. 12 Reflection and refraction of plane SV incident wave at 26.6°: (a) schematic diagram of problem; (b) numerical result

The graphical method shown in Figs. 8 and 9 for free-boundary reflection may similarly be applied to the problem of refraction, except that two different slowness surfaces, corresponding to the two different media, must be used in the left and right half planes divided by the (vertical) interface. Fig. 13 shows such a diagram, where the-axis may be regarded as the material interface. A typical case of incident P wave having the angle of incidence, θ_1, is dealt with in Fig. 13, where a qP and a qSV waves are found to be refracted with angles of refraction, θ_1'' and θ_2'', respectively. Cases of incident SV waves are more complicated, but they are not discussed in detail here because they may be handled in the same manner as in the previous subsection. An example of computed wavefield is shown in Fig. 14, which shows two refracted qSV waves (both labeled qSV) generated due to an incident SV wave of an angle of incidence, 71.6°. Such refraction behavior may be explained by

considering in Fig. 13 a case similar to the one represented by line c-c in Fig. 9. ('Line c-c' must be drawn horizontally in Fig. 13 because of the horizontal interface.)

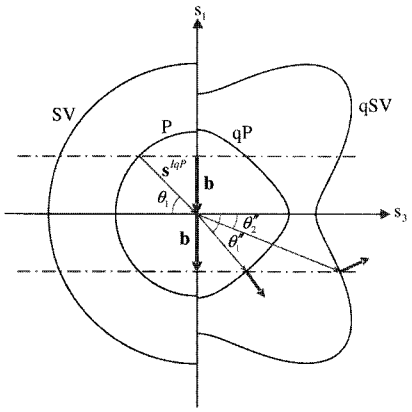

Fig. 13 Analytical determination of angles of refraction using slowness surfaces for incident qP waves

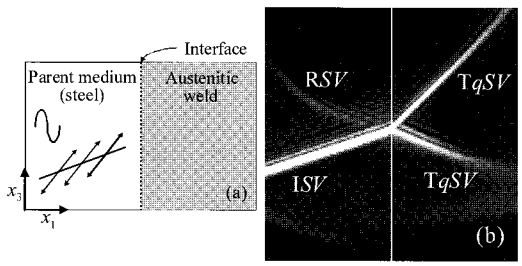

Fig. 14 Reflection and refraction of plane SV incident wave 71.6°: (a) schematic diagram of problem; (b) numerical result

From the numerical results in Figs. 11, 12 and 14, and other similar results for various angles of incidence and for incident P and SV modes, the angles of refraction have been measured. As in the case of free-boundary reflection, they have exhibited excellent agreement (that is, within up to 0.6° error) with the analytical values determined by the graphical method described above. This clearly demonstrates the capability of MSLM to predict accurately the angles of refraction of the ultrasonic waves transmitted into the anisotropic weld.

3.4 Scattering of Waves from cracks

As the last fundamental process of waves in Fig. 1, scattering of ultrasonic waves from cracks in the anisotropic weld is simulated in this subsection. Various cases of relative orientation of the incident wave with respect to a crack have been simulated, and only two of them are presented in this paper.

Figs. 15 and 16 shows the computed wavefields for incident qSV and qP waves, respectively, propagating in the directions parallel and perpendicular to a horizontal semi-infinite crack (see Figs. 15(a) and 16(a)). In both of the numerical results given in Figs. 15(b) and 16(b), diffracted qP (labeled DqP) and diffracted qSV (DqSV) waves emanating from the crack tip are clearly observed. In addition, a reflected qP wave (RqP), generated from the upper crack face, is

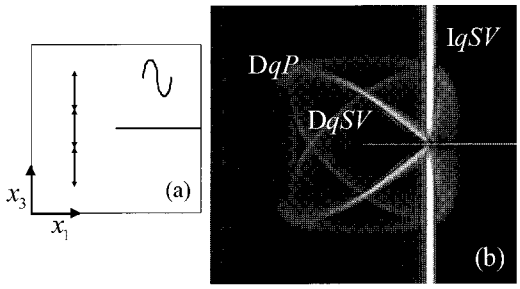

Fig. 15 Computed wavefield for incident qSV wave propagating along horizontal crack: (a) schematic diagram of problem; (b) numerical result

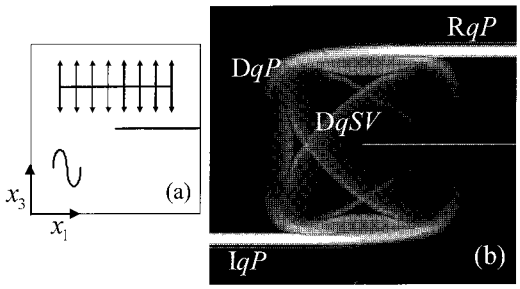

Fig. 16 Computed wavefield for incident qP wave propagating normal to horizontal crack: (a) schematic diagram of problem; (b) numerical result

observed in Fig. 16(b). Since comparable analytical solution is not readily available, only the existence of the diffracted waves centered at the crack tip has been discussed. Therefore, the MSLM may be claimed to able to correctly predict the diffraction behavior of ultrasonic waves from a crack tip at least from the qualitative point of view.

4. Simulation of Ultrasonic Inspection of a Model Weld

Combined use of the features of MSLM demonstrated so far enables the simulation of a simple ultrasonic testing problem, further simplified from the one in Fig. 1. That is, the geometry of the weld bead is simpler than in Fig. 1, and the weldment is assumed to be homogeneous.

The example problem is aimed at detecting a lack of sidewall fusion in a V-butt austenitic weld. In the schematic diagram shown in Fig. 17, the size of specimen is approximately 8.65 cm by 2.16 cm. The properties of steel are the same as before, and it is assumed that the property of the austenitic weld is uniform within the V-butt weld, which is not the case in real world.

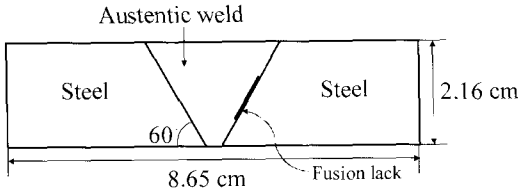

Fig. 17 Schematic diagram of a pulse-echo setup for ultrasonic testing of welds containing a lack of sidewall fusion

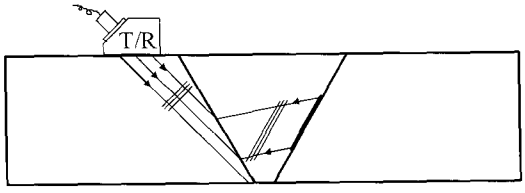

Fig. 18 Ray paths for the basic pulse-echo setup in Fig. 17

For this problem, only a basic pulse-echo scheme is considered. Fig. 18 shows ray paths for a basic pulse-echo testing of sidewall defects. All ray paths are SV or qSV waves. The rays represent energy propagation directions, with the wavefronts shown as three parallel line segments.

Simulated wavefields for such a problem at a few discrete times are shown in Fig. 19. The transmitting probe is assumed to be a 45° SV probe as simulated by the method described by Yim and Baek (2002). As shown in Fig. 19(a), a transmitting and receiving probe (often called the T/R probe) introduces 45° incident SV waves into the isotropic steel. Fig. 19(b) shows the SV incident waves transmit into the austenitic weld and Fig. 19(c) the refracted waves reflect from the lack of sidewall fusion. In Fig. 19(d), they refracted to the parent medium steel and return to the T/R probe shown in Fig. 19(e) and 19(f). Finally, the wavefield becomes very complicated in Fig. 19(f) due to the multiple reflections and refractions at the weld faces, and diffraction from the two points of the lack of sidewall fusion.

The voltage signal graph shown in Fig. 20 is obtained as a result of the numerical simulation, which shows a reflected wave signal from the fusion lack. In Fig. 20, wave packets 1 and 2 are the so-called "main bang", wave packet 3 may be identified as the diffracted SV wave from the left bottom corner of the weld, and wave packet 4 is the defect signal. It is noteworthy that the "main bang" seems to consist of two isolated wave packets because of wave cancellation in between, and that the defect signal is significantly big in this problem because the wave normal of these refracted qSV waves happen to be almost normal to the lack of fusion. The absolute value of the signal in the graph has no meaning, and only the relative values matter.

In this example, we have seen the feasibility to use the MSLM for simulating ultrasonic testing in problems involving anisotropic welds.

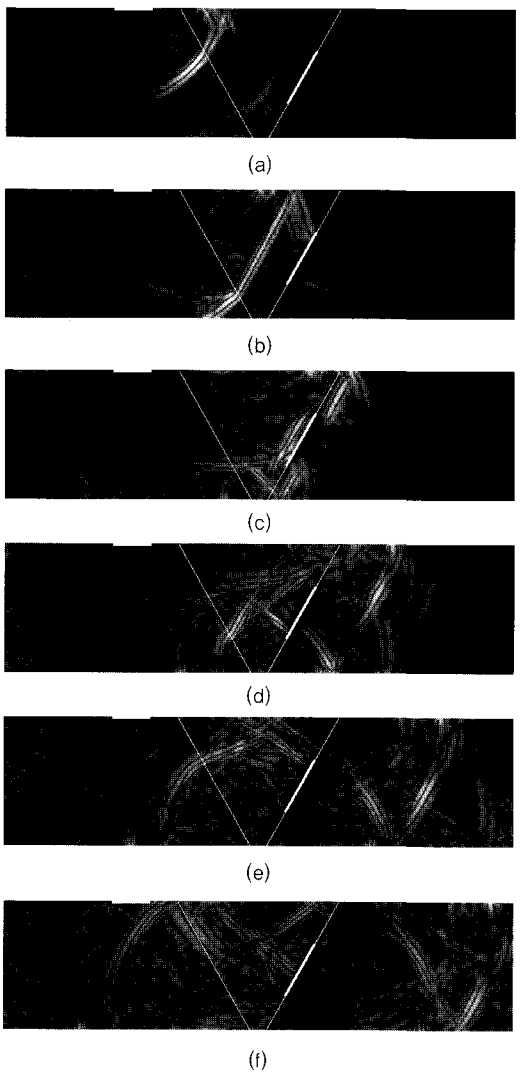

Fig. 19 Computed wavefields, at various time steps for problem in Fig. 17

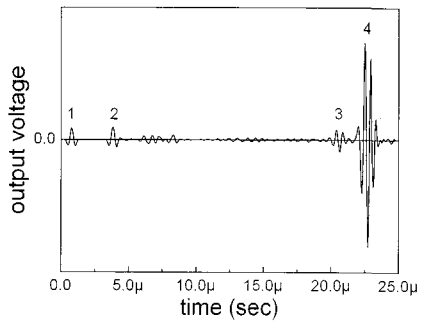

Fig. 20 A-Scan waveform for problem in Fig. 17

5. Conclusions

As a prospective and effective method to simulate ultrasonic testing of transversely isotropic austenitic welds, a version of the MSLM — a numerical model previously used for unidirectional composites — has been considered. In order to investigate the potential of the model in this application, each of the fundamental processes undergone by ultrasonic waves in a typical ultrasonic testing of an austenitic weld has been simulated.

First of all, generation of waves from point and line sources and their propagation in an unbounded anisotropic medium have been simulated. The numerical results exhibited major characteristic features of waves in anisotropic media, such as cusps on the qSV wave surface, predicted by the analytical analysis. Secondly, reflection of waves at free boundaries of the austenitic weld has been simulated for various angles of incidence and for both qP and qSV modes of the incident wave. In all cases considered, the number and modes of reflected waves and their angles of reflection have shown excellent agreement with the analytical results based on the slowness surfaces. In particular, the MSLM correctly predicted the existence and angles of two qSV reflected waves, including the so-called 'second qSV wave' (Langenberg et al., 2000). The third process considered was the transmission of plane waves into the anisotropic weld medium across a plane interface with the isotropic parent medium. Again, in all cases simulated, the number and modes of refracted waves and their angles have agreed excellently with the analytical results. In addition, wavefields scattered from cracks have been computed, and some preliminary results shown. Diffracted waves from a crack tip have been clearly observed in the numerical results as predicted by the wave mechanics.

Finally, by combining all the features of the MSLM demonstrated in the fundamental problems, the ultrasonic inspection has been successfully

simulated by using a simple 'model' of a homogeneous austenitic weld and a numerical model for an oblique SV probe. The computed wavefields in this problem have shown details of wave interaction with the weld, and also exhibited waves to be detected by the probe in the pulse-echo setup. All the results presented in this paper clearly manifest a great potential of the MSLM in the numerical modeling of ultrasonic inspection for austenitic welds. Yet, this paper is merely a presentation of preliminary results, and much more effort is required for further development of the MSLM so that it may be used to model the *actual* situation of ultrasonic austenitic weld inspection, e. g. the non-homogeneous microstructure of the weld.

Acknowledgments

This work was supported by grant No. R01-2005-000-10395-0 from the Basic Research Program of the Korea Science & Engineering Foundation, and the Safety and Structural Integrity Research Center sponsored by the Korea Science and Engineering Foundation.

References

Henneke II, E. G. (1972) Reflection-refraction of a stress wave at a plane boundary between anisotropic media, Journal of the Acoustical Society of America, Vol. 51, No. 1, pp. 210-217

Langenberg, K. J., Hannemann, R., Kaczorowski, T., Marklein, R., Koehler, B., Schurig, C., and Walte, F. (2000) Application of modeling techniques for ultrasonic austenitic weld inspection, NDT&E International, Vol. 33, pp. 465-480

Musgrave, M. J. P. (1954) On the propagation of elastic waves in aeolotropic media, Proceedings of Royal Society of London, Vol. 226, pp. 339-355

Musgrave, M. J. P. (1970) Deviation of ray from wave normal for elastic waves in principal planes of crystal symmetry, Journal of Mechanics and Physics of Solids, Vol. 18, pp. 207-211

Ogilvy, J. A. (1985) Computerized ultrasonic ray tracing in austenitic steel, NDT International, Vol. 18, No. 2, pp. 67-77

Ogilvy, J. A. (1986) Ultrasonic beam profiles and beam propagation in an austenitic weld using a theoretical ray tracing model, Ultrasonics, Vol. 24, pp. 337-347

Yamawaki, H. and Saito, H. (2000) Numerical calculation of ultrasonic propagation with anisotropy, NDT&E International, Vol. 33, pp. 489-497

Yim, H. and Choi, Y. (2000) Simulation of ultrasonic waves in various types of elastic media using the mass spring lattice model, Materials Evaluation, Vol. 58, pp. 889-896

Yim, H. and Sohn, Y. (2000) Numerical simulation and visualization of elastic waves using mass-spring lattice model, IEEE Transactions on Ultrasonics, Ferroelectrics and Frequency Control, Vol. 47, No. 3, pp. 549-558

Yim, H. and Baek, E. (2002) Two-dimensional numerical modeling and simulation of ultrasonic testing, Journal of the Korean Society for Nondestructive Testing, Vol. 22, No. 6, pp. 649-658